



Ning Liu · Wenbin Yu · Dewey H. Hodges

Mechanics of structure genome-based global buckling analysis of stiffened composite panels

Received: 2 May 2018 / Revised: 12 November 2018 / Published online: 19 December 2018
© Springer-Verlag GmbH Austria, part of Springer Nature 2018

Abstract Stiffened panels buckle under compressive loads which would degrade load-bearing capabilities of the structures. Fast yet accurate estimations of buckling loads and associated mode shapes are critical in the early stages of design and optimization. This paper presents a method based on the mechanics of structure genome (MSG) for the global buckling analysis of stiffened composite panels. The original geometrically nonlinear problem is mathematically reduced to a geometrically linear constitutive modeling of the structure genome and a geometrically nonlinear formulation of the macroscopic plate analysis. Validation case studies show that MSG is highly accurate and efficient as compared to the detailed finite element analysis. The buckling behaviors of stiffened panels under various boundary conditions and loadings are investigated.

1 Introduction

Stiffened panels have been widely used in many engineering systems. By adding stiffeners to plates, buckling strengths of the structures are significantly enhanced without significant increase in weight. Buckling analysis of stiffened panels has been a subject of interest for many years. Depending on the stiffness and patterns of stiffeners and the space between stiffeners, buckling modes are generally seen in two types: global buckling and local buckling (Fig. 1). In global modes, skins and stiffeners are lifted together, while in local modes only the skins between the stiffeners are lifted. According to the failure mode map [1], global buckling is considered to be a major failure mode for stiffened plates/shells under axial compression and/or external pressure [2] and one of the design objectives for optimization [3].

Among works on global buckling analysis of stiffened panels, extensive studies are focused on finite element method (FEM) and smeared stiffener method (SSM). The FEM enables accurate results without limitations regarding boundary conditions, stiffener shapes, or layup sequences. However, studies showed that modeling stiffeners using two-dimensional (2D) elements resulted in significant error in predicted buckling loads in comparison with using three-dimensional (3D) elements [4]. Accurate simulations of buckling of stiffened panels generally need high computational effort and long simulation time, prohibiting efficient evaluations of different configurations and materials needed for preliminary design and optimization [5].

The smearing techniques for plate and shell analysis have been summarized by Szilard [7]. The basic idea is to smear the stiffness of stiffeners into plates and compute effective plate/shell properties. The SSMs are in general computationally efficient to execute; however, most of the existing SSMs either lack precision or are restricted to stiffened panels with specific stiffened patterns or materials. The extension-bending coupling

N. Liu · W. Yu (✉)
School of Aeronautics and Astronautics, Purdue University, West Lafayette, IN 47906, USA
E-mail: wenbinyu@purdue.edu

D. H. Hodges
Daniel Guggenheim School of Aerospace Engineering, Georgia Institute of Technology, Atlanta, GA 30332, USA

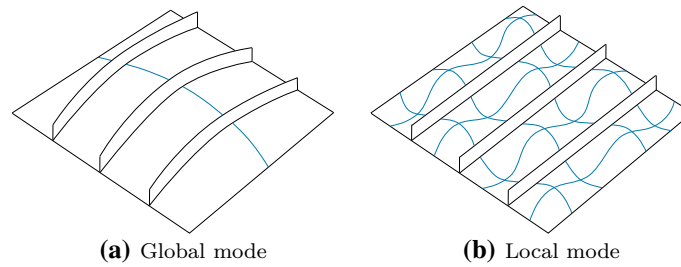


Fig. 1 Two main types of buckling modes of stiffened panels. Reprinted from [6] with permissions

interaction caused by the eccentricity of stiffeners was neglected in the study by Chen et al. [8], which resulted in imprecise predictions of the buckling behaviors [9]. The SSM proposed by Jaunky et al. [10] only applied to symmetric laminates. Byklum et al. [11] proposed an SSM to study stiffened panels with stiffeners in longitudinal and transverse directions. The resultant forces and moments were assumed to be decoupled, which made this approach difficult to use for composite panels. Kidane et al. [12] superimposed the forces and moments of stiffeners on those of shells to compute effective shell properties. The method modeled the stiffeners as Euler–Bernoulli beams without considering transverse shear stiffness, and it neglected skin–stiffener interactions. Xu et al. [13] considered the skin–stiffener interactions and proposed another SSM. This SSM was applied to various stiffened patterns but only included longitudinal moduli of stiffeners in the theory. Besides, numerical-based SSMs were developed to combine the efficiency of SSM with the accuracy of FEM [8, 14, 15]. Recently, the development of new materials such as functionally graded material (FGM) initiated active research on buckling behaviors of a stiffened FGM structures. Ninh et al. [16] studied torsional buckling and post-buckling of stiffened FGM toroidal shell. The same authors [17] also investigated dynamic buckling of a stiffened FGM toroidal shell under fluid dynamic pressure. Dung et al. [18–20] studied buckling and post-buckling of FGM truncated conical shells reinforced by orthogonal stiffeners under thermomechanical loads. Theoretical formulations in these research studies [16–20] are derived based on SSMs and classical thin shell theory with geometrical nonlinearity in the von Kármán sense.

Due to the fact that most of the SSMs are developed for specific grid-patterns or materials, applicabilities of SSMs for covering various stiffener patterns are often challenging [15]. Homogenization methods do not have such limitations regarding stiffener patterns or materials. By using the asymptotic expansion with the assumption of periodicity, all physical quantities are treated at two scales, i.e., the macroscopic scale which denotes slow variation and the microscopic scale which denotes rapid oscillations [21]. Homogenization methods have been widely used in calculating effective properties of heterogeneous media [22–24]. However, studies of using homogenization methods in buckling analysis of stiffened panels are scarce [25].

Motivated by the advantages of using homogenization theories to study buckling behaviors of stiffened panels, the authors hereby present and evaluate a homogenization theory named the mechanics of structure genome (MSG) [26]. It is a unified homogenization theory that provides the constitutive modeling of 3D structures, beams, and plates/shells [27–30]. The term genome is generalized from the representative volume element (RVE) concept in micromechanics. RVE is defined as a material volume entirely typical of the whole mixture on average and contains sufficient heterogeneity for the apparent overall properties to be effectively independent of the boundary conditions [31]. A structure genome (SG) is defined as the smallest mathematical building block of a structure (e.g., cross section of a beam, transverse normal line of a composite laminate, unit cell of a periodic structure) which can be used to compute constitutive relations for the macroscopic structural model. Particularly for stiffened panels, as shown in Fig. 2, the concept of SG enables us to decouple the original 3D problem into a constitutive modeling over the SG and a 2D plate analysis over the reference surface. Since SG is the smallest mathematical building block, SG could be a 2D domain (for blade- or hat-stiffened panels) or a 3D domain (for orthogrid- or isogrid-stiffened panels) as long as one can use the SG to mathematically build the entire structure. However, RVE will require a 3D domain for all these cases. MSG bridges the microstructure with the macroscopic structural analysis and provides a unified way to compute effective structural properties for 3D structures, beams, plates, and shells in terms of microstructures, while RVE is usually used to compute effective 3D properties. Furthermore, multiple analyses of RVE are needed for computing the complete set of properties, while only one analysis is needed for SG. More details can be found in [26], and its application to stiffened panels will be demonstrated in this paper.

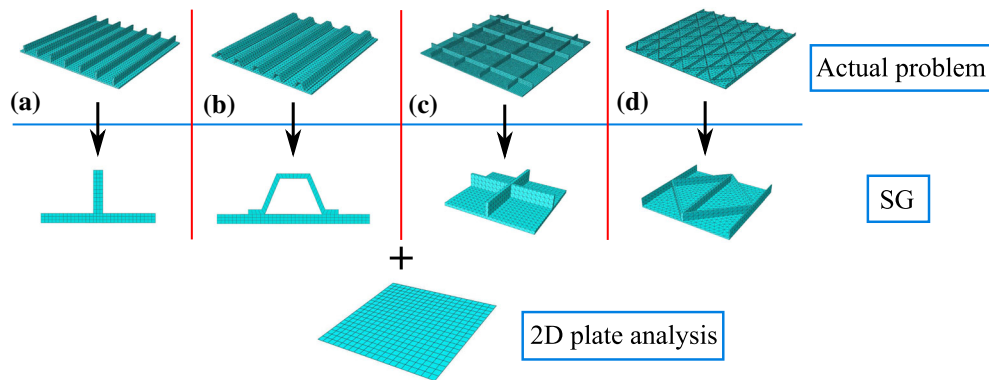


Fig. 2 Analysis of stiffened panels approximated by a constitutive modeling over the SG and a corresponding 2D plate analysis: **a** blade-stiffened panel, **b** hat-stiffened panel, **c** orthogrid-stiffened panel, **d** isogrid-stiffened panel

It should be pointed out that there are many multiscale methods in the literature. Besides the homogenization theories mentioned above [21,25,32], the multiscale finite element method (MsFEM) [33–36] also attracted significant attention. The main idea of MsFEM is to construct multiscale finite element base functions by discretizing the microstructure with a fine mesh while keeping a coarse mesh on the global domain. The construction of a base function is fully decoupled from element to element which allows MsFEM to study non-periodic structures and avoid scale separation assumption [36]. On the other hand, MSG is one of the homogenization methods which separately solve an independent constitutive modeling problem over the SG to compute effective properties as inputs for the macroscopic structural analysis. The macroscopic structural analysis can be carried out using commercial finite element packages such as ABAQUS, ANSYS, NASTRAN, etc.

The contribution of this paper is to use MSG to develop a method for the global buckling of stiffened composite panels. MSG will be used to mathematically decouple the original geometrically nonlinear problem into a linear constitutive modeling over the SG and a geometrically nonlinear analysis over the reference surface. The analysis over the reference is geometrically exact, and all the approximations in this approach are confined in the constitutive modeling. The constitutive modeling will compute the effective shell properties as inputs for ABAQUS shell elements to carry out the buckling and post-buckling analysis. With respect to papers of other authors in this field, this paper presents a unified approach to handle the global buckling and post-buckling of stiffened composite panels with the global analysis handled by traditional plate/shell elements in commercial finite element packages. This paper is organized as follows. Section 2 presents the theoretical formulation of MSG in a buckling analysis of stiffened panels. Results of validation case studies are discussed in Sect. 3. Section 4 is reserved for the conclusions.

2 MSG-based global buckling analysis of stiffened panels

We introduce macrocoordinates x_i to describe a stiffened panel, in which x_1, x_2 are in the in-plane directions and x_3 is in the normal direction. Here and throughout the paper, Latin indices take the values 1, 2, 3 except that k, l, m take 1, 2. If a plate-like structure features sufficient periods identified as SGs in the in-plane directions, and the size of SGs is much smaller than the dimensions of the macroscopic structure, we can introduce three microcoordinates $y_i = x_i/\varepsilon$ to describe the SG with ε as a small parameter. It is noted that SG has the same size as the stiffened panel in x_3 direction. The reason we also scale y_3 using ε is both y_3 and x_3 are small compared to the in-plane dimensions. The “small” parameter ε is used as a bookkeeping parameter for the asymptotic analysis needed for MSG. According to Ref. [38], the partial derivative of a function $f(x_k, y_j)$ is expressed as

$$\frac{\partial f(x_k, y_j)}{\partial x_i} = \frac{\partial f(x_k, y_j)}{\partial x_i} \Big|_{y_j=\text{const}} + \frac{1}{\varepsilon} \frac{\partial f(x_k, y_j)}{\partial y_i} \Big|_{x_k=\text{const}} \equiv f_{,i} + \frac{1}{\varepsilon} f_{i\cdot} \quad (1)$$

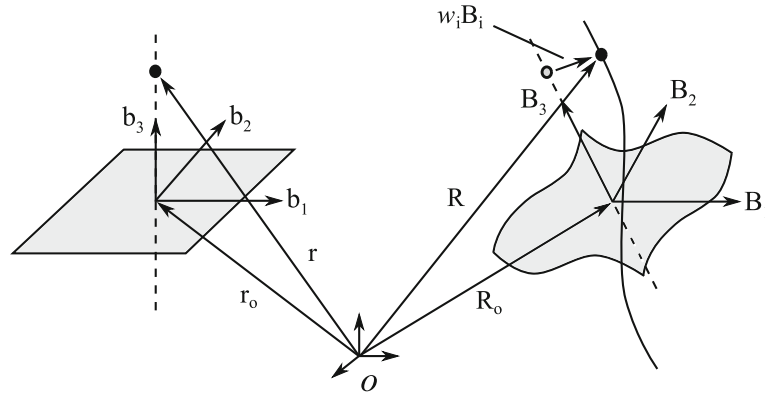


Fig. 3 Deformation of a plate structure. Reprinted from [37] with permissions

Let \mathbf{b}_k denote the unit vector tangent to x_k for the undeformed configuration, and \mathbf{b}_3 be normal to the reference surface spanned by x_k . We can describe the position of any material point of the original structure by its position vector \mathbf{r} relative to a point O fixed in an inertial frame such that

$$\mathbf{r}(x_1, x_2, y_3) = \mathbf{r}_o(x_1, x_2) + \varepsilon y_3 \mathbf{b}_3 \quad (2)$$

where \mathbf{r}_o is the position vector from O to a material point of the macroscopic plate model (Fig. 3). Because x_k is an arc-length coordinate, we have $\mathbf{b}_k = \frac{\partial \mathbf{r}_o}{\partial x_k}$.

When the original structure deforms, the particle that had position vector \mathbf{r} in the undeformed configuration now has position vector \mathbf{R} in the deformed configuration, such as

$$\mathbf{R}(x_1, x_2, y_j) = \mathbf{R}_o(x_1, x_2) + \varepsilon y_3 \mathbf{B}_3(x_1, x_2) + \varepsilon w_i(x_1, x_2, y_1, y_2, y_3) \mathbf{B}_i(x_1, x_2) \quad (3)$$

where \mathbf{R}_o denotes the position vector of the deformed macroscopic plate model, \mathbf{B}_i forms a new orthonormal triad for the deformed configuration. \mathbf{B}_i is related to \mathbf{b}_i by a direction cosine matrix, $C_{ij} = \mathbf{B}_i \cdot \mathbf{b}_j$, subject to the requirement that these two triads are the same in the undeformed configuration, and εw_i are fluctuating functions introduced to accommodate all possible deformations other than those described by \mathbf{R}_o and \mathbf{B}_i . According to Eq. (3), six constraints are needed to ensure a unique mapping to express \mathbf{R} in terms of \mathbf{R}_o , \mathbf{B}_i , and w_i . These constraints can be obtained by proper definitions of \mathbf{R}_o and \mathbf{B}_i . If we define

$$\mathbf{R}_o = \langle\langle \mathbf{R} \rangle\rangle - \langle\langle \varepsilon y_3 \rangle\rangle \mathbf{B}_3 \quad (4)$$

where $\langle\langle \cdot \rangle\rangle$ indicates averaging over the SG, we can obtain three constraints on the fluctuating functions according to Eq. (3):

$$\langle\langle w_i \rangle\rangle = 0. \quad (5)$$

The other three constraints can be obtained from \mathbf{B}_i . For a plate-/shell-like structure, we can constrain \mathbf{B}_3 so that

$$\mathbf{B}_3 \cdot \mathbf{R}_{o,1} = 0, \quad \mathbf{B}_3 \cdot \mathbf{R}_{o,2} = 0 \quad (6)$$

which implies that \mathbf{B}_3 is chosen to be normal to the reference surface of the deformed plate. It should be noted that this choice has nothing to do with the well-known Kirchhoff hypothesis. In the Kirchhoff assumption, the transverse normal can only rotate rigidly without any local deformation. However, in the present formulation, all possible deformation is allowed by classifying all deformations other than those described by \mathbf{R}_o and \mathbf{B}_i in terms of the fluctuating function $w_i \mathbf{B}_i$. The final constraint can be specified by the rotation of \mathbf{B}_k around \mathbf{B}_3 such that

$$\mathbf{B}_1 \cdot \mathbf{R}_{o,2} = \mathbf{B}_2 \cdot \mathbf{R}_{o,1}. \quad (7)$$

This constraint symmetrizes the macrostrains for a plate model as defined in Eq. (13).

According to MSG [26], for a linear elastic material characterized using a 6×6 stiffness matrix D , the strain energy can be written as

$$U = \frac{1}{2} \int \frac{1}{\omega} \langle \Gamma^T D \Gamma \rangle d\Omega \quad (8)$$

where $\Gamma = [\Gamma_{11} \ \Gamma_{22} \ \Gamma_{33} \ 2\Gamma_{23} \ 2\Gamma_{13} \ 2\Gamma_{12}]^T$ is an array containing the components of the 3D strain tensor. Ω is the domain of the macroscopic plate reference surface. The notation $\langle \bullet \rangle = \int \bullet d\omega$ is used to denote the integration over the domain of the SG, and ω denotes the volume of the domain spanned by y_k corresponding to the coordinates x_k . For plate-like structures featuring 3D SG, ω is the area of the SG in the y_1 – y_2 plane, corresponding to x_1 and x_2 remaining in the macroscopic plate model.

If we constrain ourselves to the global buckling admitted by small local rotations, the strain will be the same as the Biot strain defined in Ref. [26] according to the decomposition of the rotation tensor [39], that is

$$\Gamma = \frac{1}{2} (\mathbf{F}^T + \mathbf{F}) - \mathbf{I} \quad (9)$$

where \mathbf{F} is the deformation gradient tensor defined as

$$F_{ij} = \mathbf{B}_i \cdot \mathbf{G}_j \quad (10)$$

with \mathbf{G}_j denoting the 3D covariant base vector of the deformed configuration,

$$\mathbf{G}_k = \frac{\partial \mathbf{R}}{\partial x_k} = \frac{\partial \mathbf{R}_o}{\partial x_k} + \varepsilon y_3 \frac{\partial \mathbf{B}_3}{\partial x_k} + \varepsilon \frac{\partial w_i}{\partial x_k} \mathbf{B}_i + \varepsilon w_i \frac{\partial \mathbf{B}_i}{\partial x_k}, \quad (11)$$

$$\mathbf{G}_3 = \frac{\partial \mathbf{R}}{\partial x_3} = \mathbf{B}_3 + \frac{\partial w_i}{\partial y_3} \mathbf{B}_i. \quad (12)$$

A proper definition of the generalized strain measures for the macroscopic plate model is needed for the purpose of formulating the macroscopic plate analysis in a geometrically exact fashion. Following [40–42], we introduce the following definitions:

$$\begin{aligned} \frac{\partial \mathbf{R}_o}{\partial x_k} &= \mathbf{B}_k + \epsilon_{kl} \mathbf{B}_l, \\ \frac{\partial \mathbf{B}_i}{\partial x_k} &= \kappa_{kj} \mathbf{B}_j \times \mathbf{B}_i \end{aligned} \quad (13)$$

where ϵ_{kl} is the Lagrangian stretch tensor, κ_{kj} is the Lagrangian curvature strain tensor (or the so-called wryness tensor). This definition corresponds to the kinematics of a geometrically nonlinear Cosserat continuum [43]. If we impose the constraint given in Eq. (7), we will have the symmetry $\epsilon_{12} = \epsilon_{21}$ as a constraint for the kinematics of the plate model. This definition reproduces the 2D generalized strain measures of the Reissner–Mindlin model defined in [41]. If we further restrain \mathbf{B}_3 to be normal to the reference surface given in Eq. (6), this definition reproduces the 2D generalized strain measures of the Kirchhoff–Love plate/shell model defined in [44].

Using Eqs. (10), (11), (12), (13), the 3D strain field defined in Eq. (9) becomes

$$\begin{aligned} \Gamma_{11} &= \epsilon_{11} + \varepsilon y_3 \kappa_{11} + \underbrace{w_{1|1} + \varepsilon w_{1,1} + \varepsilon w_3 \kappa_{11} - \varepsilon w_2 \kappa_{13}}_{}, \\ \Gamma_{22} &= \epsilon_{22} + \varepsilon y_3 \kappa_{22} + \underbrace{w_{2|2} + \varepsilon w_{2,2} + \varepsilon w_3 \kappa_{22} - \varepsilon w_1 \kappa_{23}}_{}, \\ \Gamma_{33} &= w_{3|3}, \\ 2\Gamma_{23} &= \underbrace{w_{2|3} + w_{3|2} + \varepsilon w_{3,2} - \varepsilon w_1 \kappa_{21} - \varepsilon w_2 \kappa_{22}}_{}, \\ 2\Gamma_{13} &= \underbrace{w_{1|3} + w_{3|1} + \varepsilon w_{3,1} - \varepsilon w_1 \kappa_{11} - \varepsilon w_2 \kappa_{12}}_{}, \\ 2\Gamma_{12} &= \epsilon_{12} + \epsilon_{21} + \varepsilon y_3 (\kappa_{12} + \kappa_{21}) + \underbrace{w_{1|2} + w_{2|1} + \varepsilon w_{1,2} + \varepsilon w_{2,1} + \varepsilon w_3 (\kappa_{12} + \kappa_{21}) + \varepsilon w_1 \kappa_{13} - \varepsilon w_2 \kappa_{23}}_{}. \end{aligned} \quad (14)$$

Due to the smallness of ε , we neglect those underlined terms in Eq. (14) including the derivatives of fluctuating functions with respect to x_k and the products of the curvature strains and the fluctuating functions.

After dropping those underlined terms, the 3D strain field defined in Eq. (14) can be written in the following matrix form as

$$\Gamma = \Gamma_h w + \Gamma_\epsilon \bar{\epsilon} \quad (15)$$

where $w = [w_1 \ w_2 \ w_3]^T$, $\bar{\epsilon} = [\epsilon_{11} \ \epsilon_{22} \ 2\epsilon_{12} \ \kappa_{11} \ \kappa_{22} \ 2\kappa_{12}]^T$,

$$\Gamma_h = \begin{bmatrix} \frac{\partial}{\partial y_1} & 0 & 0 \\ 0 & \frac{\partial}{\partial y_2} & 0 \\ 0 & 0 & \frac{\partial}{\partial y_3} \\ 0 & \frac{\partial}{\partial y_3} & \frac{\partial}{\partial y_2} \\ \frac{\partial}{\partial y_3} & 0 & \frac{\partial}{\partial y_1} \\ \frac{\partial}{\partial y_2} & \frac{\partial}{\partial y_1} & 0 \end{bmatrix}, \quad (16)$$

and

$$\Gamma_\epsilon = \begin{bmatrix} 1 & 0 & 0 & \epsilon y_3 & 0 & 0 \\ 0 & 1 & 0 & 0 & \epsilon y_3 & 0 \\ 0 & 0 & 0 & 0 & 0 & 0 \\ 0 & 0 & 0 & 0 & 0 & 0 \\ 0 & 0 & 0 & 0 & 0 & 0 \\ 0 & 0 & 1 & 0 & 0 & \epsilon y_3 \end{bmatrix}. \quad (17)$$

According to MSG [26], the virtual work done by the applied loads can be expressed as

$$\overline{\delta W} = \int \frac{1}{\omega} \left(\langle \mathbf{p} \rangle \cdot \delta \mathbf{R} + \int_s \mathbf{Q} \cdot \delta \mathbf{R} ds \right) d\Omega \quad (18)$$

where δ is the Lagrangian variation, s denotes the boundary surfaces of the SG with applied traction force per unit area $\mathbf{Q} = Q_i \mathbf{B}_i$ and applied body force per unit volume $\mathbf{p} = p_i \mathbf{B}_i$. It should be noted that dynamic instabilities due to follower loads are beyond the scope of the current work, thus are not considered in this paper. Substituting the Lagrangian variation of the displacement field in Eq. (3) into Eq. (18), the virtual work due to the applied loads can be expressed as follows:

$$\overline{\delta W} = \overline{\delta W}_H + \epsilon \overline{\delta W}^* \quad (19)$$

where $\overline{\delta W}_H$ is the virtual work not related with the fluctuating functions w_i and $\overline{\delta W}^*$ is the virtual work related with the fluctuating functions. They are given as follows:

$$\overline{\delta W}_H = \int (f_i \overline{\delta q}_i + m_i \overline{\delta \psi}_i) d\Omega, \quad \overline{\delta W}^* = \int \frac{1}{\omega} \left(\langle p_i \delta w_i \rangle + \oint Q_i \delta w_i ds \right) d\Omega \quad (20)$$

with the generalized forces f_i and moments m_i defined as

$$f_i = \frac{1}{\omega} \left(\langle p_i \rangle + \int Q_i ds \right), \quad m_i = \frac{e_{i3j}}{\omega} \left(\langle \epsilon y_3 p_j \rangle + \int \epsilon y_3 Q_j ds \right) \quad (21)$$

where e_{i3j} is the Levi-Civita symbol. Virtual displacements $\overline{\delta q}_i$ and rotations $\overline{\delta \psi}_j$ are defined as

$$\overline{\delta q}_i = \delta \mathbf{R}_o \cdot \mathbf{B}_i, \quad \delta \mathbf{B}_3 = \overline{\delta \psi}_j \mathbf{B}_j \times \mathbf{B}_3. \quad (22)$$

The principle of minimum total potential energy states

$$\delta U = \overline{\delta W}. \quad (23)$$

In view of the strain energy in Eq. (8) and virtual work in Eq. (19), the variational statement in Eq. (23) can be rewritten as the following after dropping the virtual work related to the small parameter ϵ :

$$\int \left[\frac{1}{2\omega} \delta \langle \Gamma^T D \Gamma \rangle - (f_i \overline{\delta q}_i + m_k \overline{\delta \psi}_k) \right] d\Omega = 0. \quad (24)$$

Considering the fact that the last term in Eq. (24) is not a function of w_i , we can conclude that the fluctuating function is governed by the following variational principle:

$$\delta \frac{1}{2} \langle (\Gamma_h w + \Gamma_\epsilon \bar{\epsilon})^T D (\Gamma_h w + \Gamma_\epsilon \bar{\epsilon}) \rangle = 0. \quad (25)$$

To solve this variational statement numerically, the fluctuating function w is discretized as

$$w(x_k, y_j) = S(y_j) V(x_k) \quad (26)$$

where S denotes standard shape functions and V denotes nodal values of the fluctuating function. Substituting Eq. (26) into Eq. (25), we obtain the following discretized version of the strain energy functional:

$$U = \frac{1}{2} (V^T E V + 2V^T D_{h\epsilon} \bar{\epsilon} + \bar{\epsilon}^T D_{\epsilon\epsilon} \bar{\epsilon}). \quad (27)$$

The first term represents the contribution from the fluctuating functions, the second term represents the contribution from the interaction of the fluctuating functions and generalized plate strains, and the last term represents the strain energy due to generalized plate strains without any fluctuating functions. The corresponding coefficient matrices are defined as

$$E = \langle (\Gamma_h S)^T D (\Gamma_h S) \rangle, \quad D_{h\epsilon} = \langle (\Gamma_h S)^T D \Gamma_\epsilon \rangle, \quad D_{\epsilon\epsilon} = \langle \Gamma_\epsilon^T D \Gamma_\epsilon \rangle. \quad (28)$$

Minimizing U in Eq. (27) gives us the following linear system:

$$E V = -D_{h\epsilon} \bar{\epsilon}. \quad (29)$$

It is noted that the linear system in Eq. (29) is due to the restriction of small local rotations used to define strains in Eq. (9). Such a restriction implies that local buckling modes within an SG are excluded. It is seen that V linearly depends on $\bar{\epsilon}$; therefore, the solution can be symbolically written as

$$V = V_0 \bar{\epsilon}. \quad (30)$$

Substituting Eq. (30) back into Eq. (27), we calculate the strain energy stored in the SG as

$$U = \frac{1}{2} \bar{\epsilon}^T (V_0^T D_{h\epsilon} + D_{\epsilon\epsilon}) \bar{\epsilon} \equiv \frac{\omega}{2} \bar{\epsilon}^T \bar{D} \bar{\epsilon} \quad (31)$$

where \bar{D} is the effective 6×6 stiffness matrix (commonly called A , B , and D matrices in mechanics of composite materials) to be used in the macroscopic plate analysis. This stiffness matrix can be explicitly expressed in the following plate constitutive relation:

$$\begin{Bmatrix} N_{11} \\ N_{22} \\ N_{12} \\ M_{11} \\ M_{22} \\ M_{12} \end{Bmatrix} = \begin{bmatrix} A_{11} & A_{12} & A_{16} & B_{11} & B_{12} & B_{16} \\ A_{12} & A_{22} & A_{26} & B_{12} & B_{22} & B_{26} \\ A_{16} & A_{26} & A_{66} & B_{16} & B_{26} & B_{66} \\ B_{11} & B_{12} & B_{16} & D_{11} & D_{12} & D_{16} \\ B_{12} & B_{22} & B_{26} & D_{12} & D_{22} & D_{26} \\ B_{16} & B_{26} & B_{66} & D_{16} & D_{26} & D_{66} \end{bmatrix} \begin{Bmatrix} \epsilon_{11} \\ \epsilon_{22} \\ 2\epsilon_{12} \\ \kappa_{11} \\ \kappa_{22} \\ 2\kappa_{12} \end{Bmatrix}. \quad (32)$$

Substituting the strain energy stored in SG in Eq. (31) into Eq. (24), we can rewrite the variational statement governing the original structure as

$$\int \left[\delta \left(\frac{1}{2} \bar{\epsilon}^T \bar{D} \bar{\epsilon} \right) - f_i \delta q_i - m_k \delta \psi_k \right] d\Omega = 0. \quad (33)$$

This variational statement governs the macroscopic plate model as it only concerns the 2D field variables in terms of the macrocoordinates x_k . Therefore, the above-mentioned formulations show that a geometrically nonlinear 3D formulation defined in Eq. (23) can be mathematically reduced to a geometrically linear constitutive modeling over the SG in Eqs. (29)–(31) and a geometrically nonlinear 2D plate analysis in Eq. (33). The nonlinearity of the 2D plate analysis is due to the nonlinear generalized strains defined in Eq. (13). In other words, as an alternative to the 3D formulation, the buckling analysis of stiffened composite panels can be simplified into a constitutive modeling in SG and a buckling analysis of a 2D plate (Fig. 4). The linear constitutive modeling is implemented in a computer code named SwiftComp. The constitutive relations given in this paper are computed using SwiftComp. The linearized buckling analysis and nonlinear post-buckling analysis of the 2D plate are performed using ABAQUS in this paper.

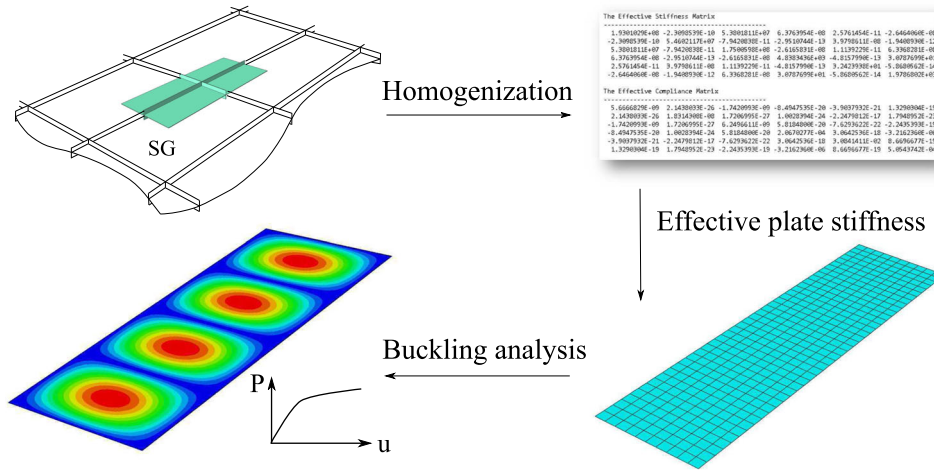


Fig. 4 Workflow of current approach: SG is homogenized to obtain the effective plate properties; the effective plate properties are defined as the general shell stiffness for 2D plate analysis; a buckling analysis is performed on the plate reference surface

3 Examples and results

In this Section, we will validate the MSG-based global buckling approach using detailed FEA using ABAQUS 20-noded brick elements with reduced integration (C3D20R). In the 2D plate analysis, an 8-noded shell element with reduced integration (S8R5) is employed. Uniaxial compressive loads are applied at the short edges; all edges are simply supported meaning that their out-of-plane deflection is constrained. The boundary conditions remain the same for the validation case studies throughout the paper unless specific changes are mentioned.

3.1 Buckling of a blade-stiffened composite panel

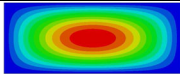
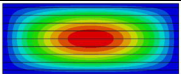
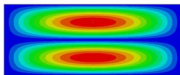
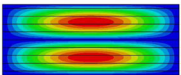
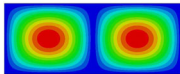
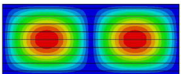
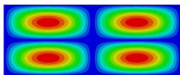
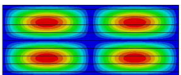
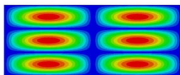
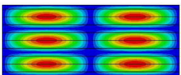
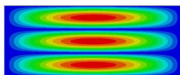
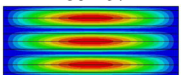
A blade-stiffened composite panel (Fig. 2) is studied to validate the current approach. The first six buckling modes and their associated buckling loads and mode shapes are compared. This stiffened plate is 6.3 m long, 2.52 m wide. Each stiffener covers 0.28-m-wide skin. The skin is 1 mm thick. The stiffeners are 20 mm tall, 3 mm thick. Laminate layup of the skin is $[0/90]_s$. Laminate layup of the stiffeners is $[(45/-45)_2 0_2]_s$. Lamina properties are $E_1 = 113$ GPa, $E_2 = E_3 = 9$ GPa, $G_{12} = G_{13} = 3.82$ GPa, $G_{23} = 3.46$ GPa, $\nu_{12} = \nu_{13} = \nu_{23} = 0.302$.

The effective plate properties, i.e., the A , B , and D matrices, are computed using MSG and are given in Table 1. The first six buckling loads and associated mode shapes are presented in Table 2. It is seen that the critical loads in the current solution are highly accurate compared with the detailed FEA results with errors less than 2%. To visualize the difference between predicted buckling mode shapes and detailed FEA, an image analysis is carried out by comparing the intensity value of each pixel in corresponding grayscale images of the contour plots that contained values in the range 0 (black) to 1 (white). The difference of the intensity value of pixels is shown in Fig. 5. It is found that the vast majority of the area in these contour plots is in complete agreement showing the high accuracy of the current method in predicting buckling mode shapes.

Table 1 The effective plate properties (A , B , and D matrices) of the blade-stiffened composite plate, units: SI

7.1591×10^7	2.7382×10^6	0	-2.6171×10^4	-5.0719×10^3	0
	6.1469×10^7	0	-5.0719×10^3	-1.1389×10^5	0
		3.8424×10^6	0	0	-7.0551×10^3
			1.3147×10^3	9.6382	0
				212.8817	0
					16.7350
	sym.				

Table 2 Comparison of first six buckling loads (N) and associated mode shapes in the case of the blade-stiffened composite plate

Mode number	Current approach	Detailed FEA	Error (%)
1	 929.63	 931.45	- 0.20
2	 1798.90	 1809.11	- 0.56
3	 3348.32	 3300.98	1.43
4	 3742.96	 3698.59	1.20
5	 4835.88	 4801.57	0.71
6	 5009.26	 5034.19	- 0.50

Mesh is removed for a clear view

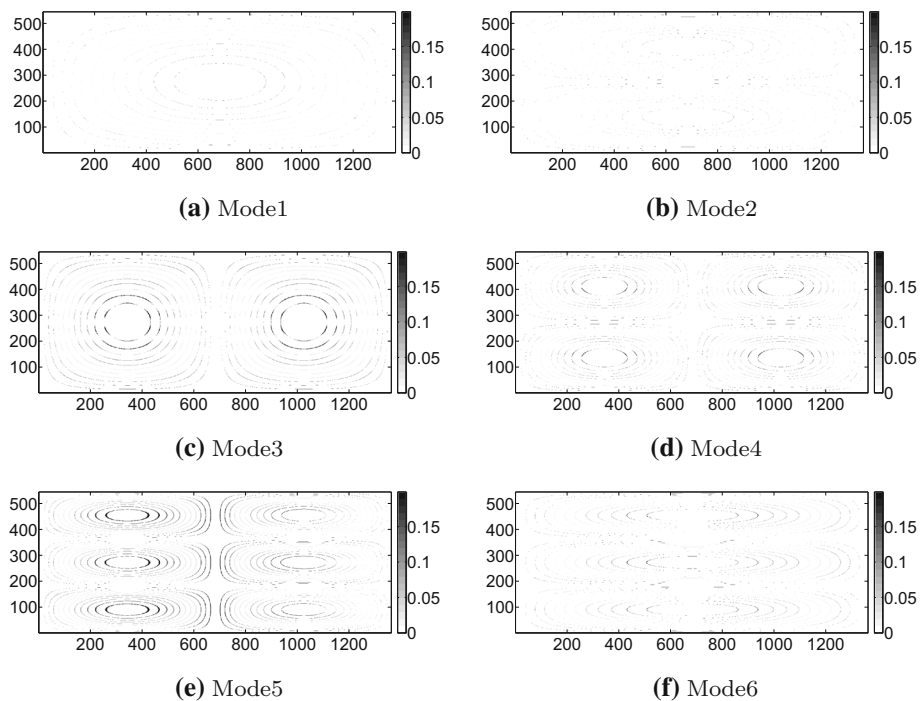


Fig. 5 Comparison of the intensity value of each pixel in corresponding grayscale images of the contour plots showing the difference between predicted buckling mode shapes and detailed FEA for the first six buckling modes. The horizontal and vertical axes are the X–Y coordinates of the pixels

3.2 Buckling under various boundary conditions and loadings

Buckling behaviors of un-stiffened plates under various boundary conditions (BCs) and loadings are studied in [45–48]. However, studies of buckling behaviors of stiffened plates under various BCs and loadings are few [49]. Motivated by this fact, the authors carry out a study in which buckling behaviors of stiffened panels under selective BCs and loadings are investigated.

We use the same stiffened panel studied in Sect. 3.1. Typical combinations of different BCs are shown in Fig. 6. The naming convention starts with the pair of BCs on the vertical edges followed by the pair of BCs on the horizontal edges [50]. For those stiffened panels with BCs defined in Fig. 6, only uniform uniaxial compressive loads are applied at vertical edges. The studied loading conditions are shown in Fig. 7. The stiffened panels under these loading conditions are simply supported. The critical load can be expressed in general as follows [49]:

$$N = \int \lambda \left(1 - \alpha \frac{y}{b}\right) dy \tag{34}$$

where λ is the critical stress, $\alpha = 0$ indicates uniform uniaxial loading, $\alpha = 1$ indicates linearly varying uniaxial loading starting from zero, and b is the width of the edges where loads apply.

Critical buckling loads and associated mode shapes under various BCs and loadings are presented in Table 3. It is expected that the critical buckling loads increase as the BCs make the structure stiffer. It is also observed that clamping the loading edges will significantly increase the buckling loads. CCSS BCs almost double the buckling loading compared with CSCS BCs. Different loading conditions also affect critical buckling loads. The biaxial loading state results in a much lower critical load (255.38 N) as opposed to the uniform uniaxial

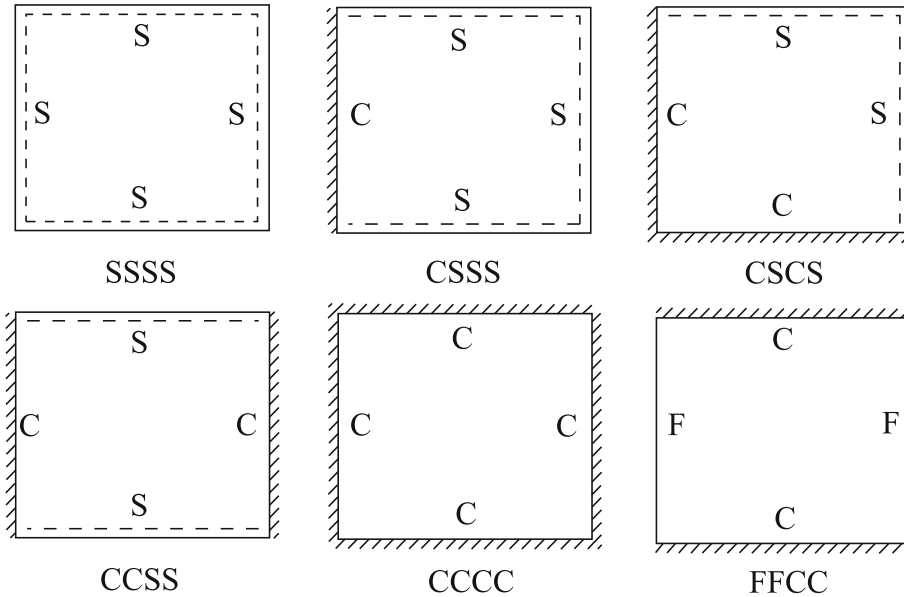


Fig. 6 Typical combinations of different boundary conditions (S: simply supported, C: clamped, F: free)

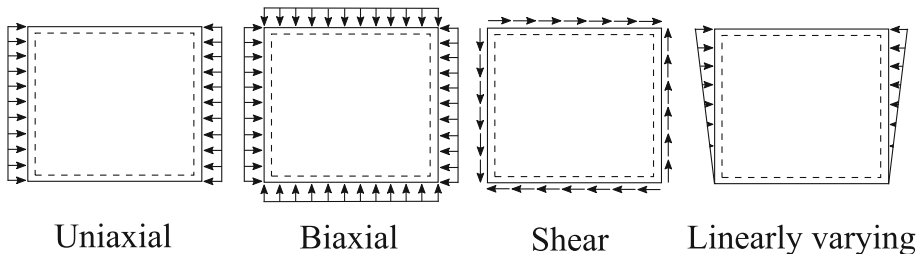
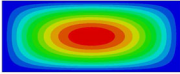
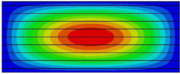
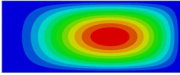
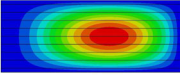
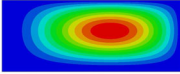
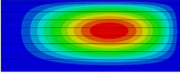
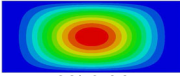
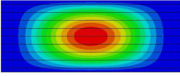
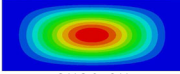
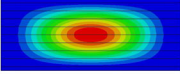
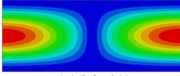
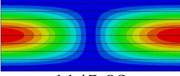
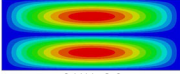
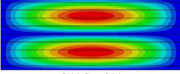
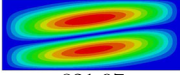
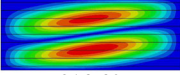
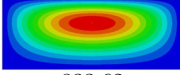
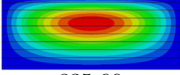


Fig. 7 Typical loading conditions

Table 3 Investigation of critical buckling of the blade-stiffened composite panel under different boundary conditions and loadings

BCs/loading	Current approach	Detailed FEA	Error (%)
SSSS	 929.63	 931.45	- 0.20
CSSS	 1779.30	 1772.86	0.36
CSCS	 1843.41	 1839.16	0.23
CCSS	 3378.06	 3339.13	1.15
CCCC	 3539.85	 3505.11	0.98
FFCC	 1130.95	 1145.93	- 1.32
Biaxial	 255.38	 258.45	- 1.19
Shear	 821.97	 816.69	0.65
L.V.	 833.62	 835.66	- 0.24

Loads are in Newton; L.V. is linearly varying uniaxial loading; mesh is removed for a clear view

loading state (929.63 N). Under shear loading, the stiffened panel falls into an overall shear pattern without significant shear deformation seen in the skin between stiffeners. This is mainly due to the tightness of the space between stiffeners. The required buckling load under linearly varying uniaxial loading (833.62 N) is less than the critical load under uniform uniaxial loading (929.63 N) due to the fact that the structure is not loaded evenly. An image analysis (Fig. 8) shows good agreement between predicted buckling mode shapes and detailed FEA results.

3.3 Post-buckling analysis

The accuracy of the current approach in predicting the post-buckling behavior of a stiffened composite plate is investigated in this Section. Post-buckling is referred to the behavior after the buckling of the plate takes place. ABAQUS Riks method [51,52] is used in the current work to predict the nonlinear post-buckling behavior of stiffened composite plates. Same example studied in Sect. 3.1 is used in this study.

The procedure to perform a post-buckling analysis for both detailed FEA and the current approach is the same and stated as follows. The first three buckling modes are selected to construct imperfections. The associated imperfection sizes (i.e., imperfection scaling factors) are assumed to be 2×10^{-4} , 1×10^{-4} , 0.5×10^{-4} . Results are predicted using 400 iteration steps, minimum arc length of 1×10^{-8} and maximum arc length of 0.1. It is noted that the current work is only concerned with the elastic post-buckling behavior without considering material yielding, the study of crippling of stiffened plates is a future topic of research.

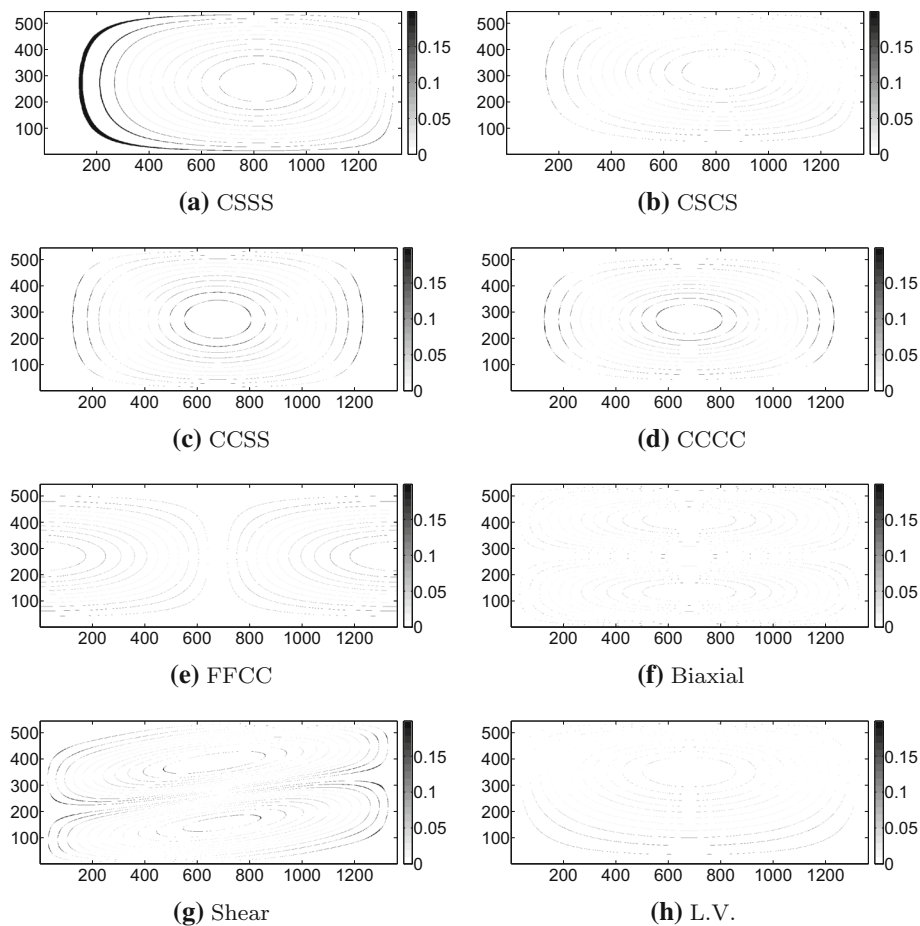


Fig. 8 Comparison of the intensity value of each pixel in corresponding grayscale images of the contour plots showing the difference between predicted buckling mode shapes and detailed FEA for different boundary conditions and loadings. The horizontal and vertical axes are the X – Y coordinates of the pixels

Load–displacement curves are compared in Fig. 9. In the Figure, the vertical axis is the normalized uniaxial load with P_{cr} as the critical buckling load; the horizontal axis is the axial shortening which is measured at the geometric center of the end cross section. It is seen that the load–displacement curve of current approach agrees very well with the curve of detailed FEA. Modeling cost and computing time are compared in Table 4. Regarding computational efficiency, the current approach is more cost-efficient than detailed FEA in modeling: 1575 shell elements (S8R5) in total as opposed to 411,804 solid elements (C3D20R) in total. The current approach is also more time-efficient than detailed FEA in performing a post-buckling analysis: 18 min with one CPU as opposed to nearly 4 days with 32 CPUs. The computational time consumed in detailed FEA could be reduced by using shell elements, but the accuracy of such solution would be significantly compromised [4]. In a nutshell, comparing with the detailed FEA, the current approach significantly reduces the computational efforts yet achieves high accuracy. For scholars who are interested in the details of the workstation on which the detailed FEA is run, they are given as follows: Dell Precision Tower 7910 powered by Intel Xeon CPU E5-2697 v3 with clock rate 2.60 GHz and 256 GB RAM.

3.4 Buckling of orthogrid- and isogrid-stiffened composite plates

To validate the current approach in the buckling analysis of other stiffened composite plates, two examples of stiffened plates from Ref. [25] are studied. Their geometries, materials, and stiffened patterns are reiterated as follows. Two flat plates with the length of 4.3764 m and the width of 1.5024 m are stiffened on one side by orthogrid and isogrid stiffeners, respectively, as shown in Fig. 2. Dimensions of an SG in the orthogrid are

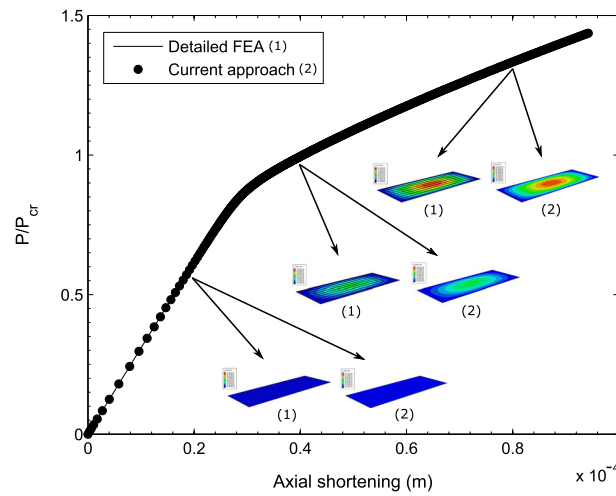


Fig. 9 Comparison of post-buckling load–displacement curve between current approach and detailed FEA

Table 4 Comparison of computational cost to perform post-buckling analysis between current approach and detailed FEA

	Current approach	Detailed FEA
Element type	Shell (S8R5)	Solid (C3D20R)
Total element number	1575	411,804
CPU number	1	32
Computational time	18 min	3 days 20 h

Table 5 The effective plate properties (A , B , and D matrices) of the orthogrid-stiffened plate, units: SI

1.2021×10^8	2.4210×10^7	0	2.1300×10^5	-2.0466×10^4	0
	9.6465×10^7	0	-2.0511×10^4	6.5780×10^4	0
		2.5376×10^7	0	0	-2.2878×10^4
			2.4269×10^3	35.152	0
	sym.			1.1915×10^3	0
					26.548

0.10941 m long by 0.040095 m wide; dimensions of an SG in the isogrid are 0.236562 m long by 0.13658 m wide. The angles between stiffeners in the isogrid are 60° . The skin laminate has an eight-ply symmetric layup of $[\pm 45/90/0]_s$, with each ply thickness equal to 0.1524 mm. The lamina properties are $E_1 = 139.31$ GPa, $E_2 = E_3 = 13.103$ GPa, $G_{12} = G_{13} = G_{23} = 5.0345$ GPa, $\nu_{12} = \nu_{13} = \nu_{23} = 0.3$. All the stiffeners are made of 0° material with a height of 12.9 mm and a width of 1.524 mm. Uniaxial compressive loads are applied to the short edges, and all edges are simply supported meaning that their out-of-plane deflection is constrained. The effective plate properties (A , B , and D matrices) of two examples are given in Tables 5 and 6.

Critical buckling loads and mode shapes predicted by current approach are compared with the results from Ref. [25] in Table 7. It is seen that the results of the current approach are very close to Ref. [25] and the detailed FEA, which illustrates the high accuracy of the current method in predicting the global buckling loads of stiffened panels with various grid-patterns.

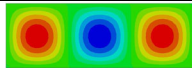
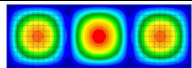
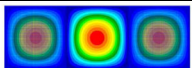
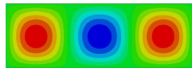
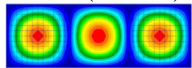
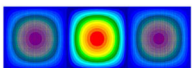
4 Conclusions

A homogenization theory, namely the mechanics of structure genome, is presented and evaluated in studying the global buckling behavior of stiffened composite panels. The linearized buckling loads, associated mode shapes, as well as post-buckling load–displacement curves under various boundary conditions and loadings are assessed. A geometrically nonlinear buckling analysis is mathematically reduced to a geometrically linear

Table 6 The effective plate properties (A , B , and D matrices) of the isogrid-stiffened plate, units: SI

9.8845×10^7	3.2062×10^7	-1.0371×10^5	-1.8535×10^5	-5.8541×10^4	-457.46
	1.0053×10^8	-3.57691×10^4	-5.8523×10^4	-1.7879×10^5	-166.00
		3.3451×10^7	-454.66	-164.65	-6.3335×10^4
			1.5959×10^3	523.23	0
	sym.			1.6431×10^3	0
					541.47

Table 7 Comparison of critical buckling load and mode shape of the orthogrid- and isogrid-stiffened composite panels

	Current approach	Wang et al. [25]	Detailed FEA [25]
Orthogrid	 16.80 (- 0.53%)	 16.85 (- 0.24%)	 16.89
Anglegrid	 23.80 (0.85%)	 24.67 (4.53%)	 23.60

Loads are in N/mm. Pictures from [25] are reprinted with permissions

constitutive modeling of the SG and a geometrically nonlinear buckling analysis of the macroscopic plate. The effective plate properties (A , B , and D matrices) are computed by the constitutive modeling, and the buckling behaviors of the stiffened composite panels are approximated by a buckling analysis of the homogeneous plates with the effective plate properties. Validation case studies show that this approach is highly accurate in the buckling and post-buckling analysis of stiffened composite panels for various grid-patterns and boundary conditions. This approach is also highly time-efficient in the post-buckling analysis of stiffened composite panels in comparison with detailed FEA. The current work is part of a continued study in global and local buckling analysis of stiffened composite panels using MSG. The local buckling behavior is going to be predicted by a geometrically nonlinear constitutive modeling of the SG in a future study. The present approach can be incorporated into any design and optimization methodologies of stiffened composite panels for fast and accurate predictions of the global buckling behavior of stiffened panels.

References

- Zheng, Q., Jiang, D., Huang, C., Shang, X., Ju, S.: Analysis of failure loads and optimal design of composite lattice cylinder under axial compression. *Compos. Struct.* **131**, 885 (2015)
- Lopatin, A., Morozov, E.: Buckling of the composite sandwich cylindrical shell with clamped ends under uniform external pressure. *Compos. Struct.* **122**, 209 (2015)
- Wodesenbet, E., Kidane, S., Pang, S.S.: Optimization for buckling loads of grid stiffened composite panels. *Compos. Struct.* **60**(2), 159 (2003)
- Fenner, P.E.: Finite element buckling analysis of stiffened plates with filleted junctions. *Thin-Walled Struct.* **59**, 171 (2012)
- Bisagni, C., Vescovini, R.: Analytical formulation for local buckling and post-buckling analysis of stiffened laminated panels. *Thin-Walled Struct.* **47**(3), 318 (2009)
- Stamatelos, D., Labeas, G., Tserpes, K.: Analytical calculation of local buckling and post-buckling behavior of isotropic and orthotropic stiffened panels. *Thin-Walled Struct.* **49**(3), 422 (2011)
- Szilar, R.: *Theories and Applications of Plate Analysis: Classical Numerical and Engineering Methods*. Wiley, Hoboken (2004)
- Chen, H.J., Tsai, S.W.: Analysis and optimum design of composite grid structures. *J. Compos. Mater.* **30**(4), 503 (1996)
- Sadeghifar, M.: Buckling analysis of stringer-stiffened laminated cylindrical shells with nonuniform eccentricity. *Arch. Appl. Mech.* **81**(7), 875 (2011)
- Jaunky, N., Knight, N.F., Ambur, D.R.: Formulation of an improved smeared stiffener theory for buckling analysis of grid-stiffened composite panels. *Compos. Part B* **27**(5), 519 (1996)
- Byklum, E., Steen, E., Amdahl, J.: A semi-analytical model for global buckling and postbuckling analysis of stiffened panels. *Thin-Walled Struct.* **42**(5), 701 (2004)

12. Kidane, S., Li, G., Helms, J., Pang, S.S., Woldeesenbet, E.: Buckling load analysis of grid stiffened composite cylinders. *Compos. Part B* **34**(1), 1 (2003)
13. Xu, Y., Tong, Y., Liu, M., Suman, B.: A new effective smeared stiffener method for global buckling analysis of grid stiffened composite panels. *Compos. Struct.* **158**, 83 (2016)
14. Ren, M., Li, T., Huang, Q., Wang, B.: Numerical investigation into the buckling behavior of advanced grid stiffened composite cylindrical shell. *J. Reinf. Plast. Compos.* **33**(16), 1508 (2014)
15. Wang, B., Tian, K., Hao, P., Zheng, Y., Ma, Y., Wang, J.: Numerical-based smeared stiffener method for global buckling analysis of grid-stiffened composite cylindrical shells. *Compos. Struct.* **152**, 807 (2016)
16. Ninh, D.G., Bich, D.H., Kien, B.H.: Torsional buckling and post-buckling behavior of eccentrically stiffened functionally graded toroidal shell segments surrounded by an elastic medium. *Acta Mech.* **226**(10), 3501 (2015)
17. Bich, D.H., Ninh, D.G.: Research on dynamical buckling of imperfect stiffened three-layered toroidal shell segments containing fluid under mechanical loads. *Acta Mech.* **228**(2), 711 (2017)
18. Dung, D., Nga, N.: Buckling and postbuckling nonlinear analysis of imperfect FGM plates reinforced by FGM stiffeners with temperature-dependent properties based on TSDT. *Acta Mech.* **227**(8), 2377 (2016)
19. Dung, D., Hoai, B., Hoa, L.: Postbuckling nonlinear analysis of FGM truncated conical shells reinforced by orthogonal stiffeners resting on elastic foundations. *Acta Mech.* **228**(4), 1457 (2017)
20. Chan, D., Dung, D., Hoa, L.: Thermal buckling analysis of stiffened FGM truncated conical shells resting on elastic foundations using FSDT. *Acta Mech.* **229**(5), 2221 (2018)
21. Hassani, B., Hinton, E.: A review of homogenization and topology optimization I: homogenization theory for media with periodic structure. *Comput. Struct.* **69**(6), 707 (1998)
22. Kwon, Y.W., Allen, D.H., Talreja, R.: *Multiscale Modeling and Simulation of Composite Materials and Structures*. Springer, New York (2008)
23. Kalamkarov, A.L., Andrianov, I.V., Danishevs'kyy, V.V.: Asymptotic homogenization of composite materials and structures. *Appl. Mech. Rev.* **62**(3), 030802 (2009)
24. Challagulla, K., Georgiades, A., Kalamkarov, A.: Asymptotic homogenization modeling of smart composite generally orthotropic grid-reinforced shells: part I theory. *Eur. J. Mech. A Solids* **29**(4), 530 (2010)
25. Wang, D., Abdalla, M.M.: Global and local buckling analysis of grid-stiffened composite panels. *Compos. Struct.* **119**, 767 (2015)
26. Yu, W.: A unified theory for constitutive modeling of composites. *J. Mech. Mater. Struct.* **11**(4), 379 (2016)
27. Liu, X., Yu, W.: A novel approach to analyze beam-like composite structures using mechanics of structure genome. *Adv. Eng. Softw.* **100**, 238 (2016)
28. Peng, B., Goodsell, J., Pipes, R.B., Yu, W.: Generalized free-edge stress analysis using mechanics of structure genome. *J. Appl. Mech.* **83**(10), 101013 (2016)
29. Liu, N., Yu, W.: Evaluation of smeared properties approaches and mechanics of structure genome for analyzing composite beams. *Mech. Adv. Mater. Struct.* **25**, 1–15 (2017)
30. Rouf, K., Liu, X., Yu, W.: Multiscale structural analysis of textile composites using mechanics of structure genome. *Int. J. Solids Struct.* **89**, 136–137 (2018)
31. Hill, R.: Elastic properties of reinforced solids: some theoretical principles. *J. Mech. Phys. Solids* **11**, 357 (1963)
32. Zhang, D., Waas, A.M.: A micromechanics based multiscale model for nonlinear composites. *Acta Mech.* **225**(4–5), 1391 (2014)
33. Allaire, G., Brizzi, R.: A multiscale finite element method for numerical homogenization. *Multiscale Model. Simul.* **4**(3), 790 (2005)
34. Yang, D., Zhang, H., Zhang, S., Lu, M.: A multiscale strategy for thermo-elastic plastic stress analysis of heterogeneous multiphase materials. *Acta Mech.* **226**(5), 1549 (2015)
35. Efendiev, Y., Hou, T.Y.: *Multiscale Finite Element Methods Theory and Applications*. Springer, Berlin (2009)
36. Hou, T., Wu, X.H.: A multiscale finite element method for elliptic problems in composite materials and porous media. *J. Comput. Phys.* **134**(1), 169 (1997)
37. Yu, W., Hodges, D.H., Volovoi, V.V.: Asymptotic construction of Reissner-like composite plate theory with accurate strain recovery. *Int. J. Solids Struct.* **39**(20), 5185 (2002)
38. Bensoussan, A., Lions, J.L., Papanicolaou, G.: *Asymptotic Analysis for Periodic Structures*. Studies in Mathematics and its Applications. AMS Chelsea Publishing, Providence (1978)
39. Danielson, D.A., Hodges, D.H.: Nonlinear beam kinematics by decomposition of the rotation tensor. *J. Appl. Mech.* **54**(2), 258 (1987)
40. Yu, W., Hodges, D.H., Ho, J.C.: Variational asymptotic beam sectional analysis: an updated version. *Int. J. Eng. Sci.* **59**, 40 (2012)
41. Yu, W., Hodges, D.H.: A geometrically nonlinear shear deformation theory for composite shells. *J. Appl. Mech.* **71**(1), 1 (2004)
42. Pietraszkiewicz, W., Eremeyev, V.: On natural strain measures of the non-linear micropolar continuum. *Int. J. Solids Struct.* **46**(3), 774 (2009)
43. Cosserat, E., Cosserat, F., et al.: *Théorie des corps déformables* (1909)
44. Yu, W., Hodges, D.H., Volovoi, V.V.: Asymptotic generalization of Reissner–Mindlin theory: accurate three-dimensional recovery for composite shells. *Comput. Methods Appl. Mech. Eng.* **191**(44), 5087 (2002)
45. Lopatin, A., Morozov, E.: Buckling of the SSCF rectangular orthotropic plate subjected to linearly varying in-plane loading. *Compos. Struct.* **93**(7), 1900 (2011)
46. Shufrin, I., Rabinovitch, O., Eisenberger, M.: Buckling of symmetrically laminated rectangular plates with general boundary conditions: a semi-analytical approach. *Compos. Struct.* **82**(4), 521 (2008)
47. Mezziane, M.A.A., Abdelaziz, H.H., Tounsi, A.: An efficient and simple refined theory for buckling and free vibration of exponentially graded sandwich plates under various boundary conditions. *J. Sandw. Struct. Mater.* **16**(3), 293 (2014)

-
48. Panda, S.K., Ramachandra, L.: Buckling of rectangular plates with various boundary conditions loaded by non-uniform inplane loads. *Int. J. Mech. Sci.* **52**(6), 819 (2010)
 49. Hamedani, S.J., Ranji, A.R.: Buckling analysis of stiffened plates subjected to non-uniform biaxial compressive loads using conventional and super finite elements. *Thin-Walled Struct.* **64**, 41 (2013)
 50. Reddy, J.N.: *Mechanics of Laminated Composite Plates and Shells: Theory and Analysis*, 2nd edn. CRC Press, Boca Raton (2004)
 51. Riks, E.: The application of Newton's method to the problem of elastic stability. *J. Appl. Mech.* **39**(4), 1060 (1972)
 52. Riks, E.: Some computational aspects of the stability analysis of nonlinear structures. *Comput. Methods Appl. Mech. Eng.* **47**(3), 219 (1984)

Publisher's Note Springer Nature remains neutral with regard to jurisdictional claims in published maps and institutional affiliations.